

Observation of period doubling and chaos in spin-wave instabilities in yttrium iron garnet

George Gibson and Carson Jeffries

*Department of Physics, University of California, Berkeley, California 94720
and Materials and Molecular Research Division, Lawrence Berkeley Laboratory, University of California,
Berkeley, California 94720*

(Received 11 October 1983)

Ferromagnetic resonance in a polished 0.047-cm-radius sphere of gallium-doped yttrium iron garnet is studied at 1.3 GHz in a magnetic field of 460 G. A second-order Suhl instability is observed, owing to the nonlinear coupling of the precessing uniform magnetization with spin waves. This is detected by the onset of auto-oscillations of the magnetization. One of these modes with frequency ≈ 16 kHz corresponds to the lowest spherical dimensional resonance of a packet of spin waves of small wave vector and long lifetime ($\approx 10^3$ cycles). From real-time signals, spectral analysis, and return maps this mode is found to display chaotic dynamics as the driving rf field is increased: thresholds for the onset of period-doubling bifurcations, chaos, and periodic windows. Some observed return maps bear resemblance to the two-dimensional area-preserving quadratic map of Hénon. The system has several attractors and displays "solid-state turbulence," analogous to that in fluids.

I. INTRODUCTION

Earlier, Damon¹ and Wang and Bloembergen² observed that ferromagnetic resonance in some ferrites displays premature saturation and low-field subsidiary resonance when excited above a critical value of the rf driving field H_1 . This was explained by Suhl,³ who developed a detailed theory of nonlinear coupling between the uniform precession mode of the magnetization vector and spin waves. He showed that the uniform precession could excite spin waves, whose amplitude grows essentially exponentially at a critical value of H_1 —this is the Suhl instability. He writes³ "... this situation bears a certain resemblance to the turbulent state in fluid dynamics..." This prescient comment was followed by the observation of low-frequency (10^4 – 10^6 Hz) noisy "auto-oscillations" of the magnetization,^{4–7} believed to be due to excitation of spin waves but not fully understood.

From the more recent perspective of nonlinear dynamics,⁸ one is tempted to interpret these experimental results as examples of chaotic dynamics. To this end we have experimentally reexamined the auto-oscillations in spheres of gallium-doped yttrium iron garnet (Ga-YIG), keeping in mind the routes to chaos observed in some other driven nonlinear systems.^{9–12} Using the precessing magnetization $M(t)$ as the dynamical variable and the driving field H_1 as the control parameter, we observe real-time signals, power spectra, and return maps of the system. We find period-doubling bifurcations, onset of chaos, and periodic windows. The system displays "solid-state turbulence." Of interest is the fact that for some auto-oscillation modes, the return map can be qualitatively understood (but not necessarily uniquely) by a two-dimensional quadratic map of the form given by Hénon¹³ for the nearly conservative case; this is consistent with the observation that this auto-oscillation mode has a long relaxation time.

II. EXPERIMENTAL ARRANGEMENT

Figure 1 shows the experimental arrangement used: A Ga-YIG sphere of radius R is wound with a pick-up coil

and a driving coil at right angles, providing a field H_1 at the sphere from an oscillator of frequency f_0 and variable voltage V_{rf} . This assembly is mounted in a magnetic field H_{dc} along a third, mutually perpendicular axis, which provides the Zeeman field for ferromagnetic resonance, observed from the voltage induced into the pick-up coil by the sample magnetization $\vec{M}(t)$, precessing about H_{dc} . A signal voltage V_s is obtained from diode rectification of the induced voltage. A low-frequency (100 Hz) modulation field $H_m(t)$, parallel to H_{dc} , is used to sweep through the resonance field to display the signal voltage V_s as a function of the field, i.e., ferromagnetic resonance absorption. To observe auto-oscillations of $M(t)$ we observe $V_s(t)$ at some fixed value of H_{dc} with $H_m(t) = 0$.

The Ga-YIG spheres were highly spherical (to within $\Delta R/R = 6 \times 10^{-5}$) and highly polished (to $0.15 \mu\text{m}$). Typical parameters used are radius $R = 0.047$ cm, satura-

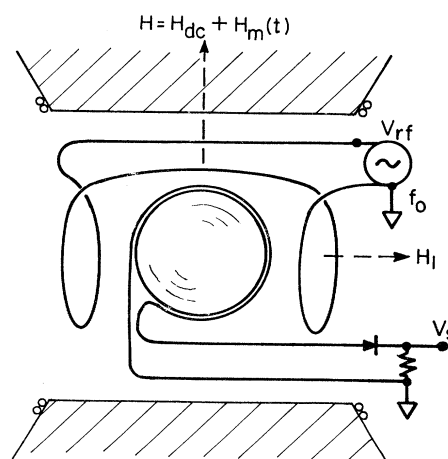


FIG. 1. Experimental arrangement showing a Ga-YIG sphere subjected to an rf field H_1 at $f_0 = 1.3$ GHz and a dc field $H_{dc} \approx 460$ Oe. A pickup coil generates a signal V_s proportional to the time derivative of the transverse magnetization of the sample.

tion magnetization $4\pi M_s = 300$ G $f_0 = 1.3$ GHz, $H_{dc} \cong 460$ G, resonance linewidth ≈ 0.5 G. Use of Ga-YIG with lower saturation magnetization allowed the use of lower resonance fields and frequencies than pure YIG.

All experiments reported here were done at room temperature and with the perpendicular pumping configuration ($\vec{H}_1 \perp \vec{H}_{dc}$) of Fig. 1. Although preliminary parallel pumping ($\vec{H}_1 \parallel \vec{H}_{dc}$) was attempted, no chaotic dynamics were observed, possibly because of insufficient pumping power available.

III. REVIEW OF SPIN-WAVE THEORY (REF. 14)

For a set of spins \vec{S}_j on a lattice in an external magnetic field \vec{H}_0 , an appropriate Hamiltonian is

$$\mathcal{H} = \gamma \hbar \sum_j \vec{H}_0 \cdot \vec{S}_j - \left[\frac{D}{Sa^2} \right] \gamma \hbar \sum_j \vec{S}_j \cdot \vec{S}_{j+1} + \mathcal{H}_{dd}. \quad (1)$$

The first term is the Zeeman interaction (γ is the gyromagnetic ratio), the second is the Heisenberg exchange interaction (D is the exchange constant, a is the lattice spacing), the last term is the dipole-dipole interaction. The Zeeman interaction gives rise to a uniform precession of the sample magnetization \vec{M} about \vec{H}_0 at the Kittel frequency,¹⁵ which for a spherical sample is $\omega_0 = \gamma H_0$. The second term leads to spin waves of frequency ω_k and wave vector k , described by the dispersion relation¹⁶

$$\omega_k^2 = \left[\omega_0 - \frac{\omega_M}{3} + \gamma D k^2 \right] \times \left[\omega_0 - \frac{\omega_M}{3} + \gamma D k^2 + \omega_M \sin^2 \theta_k \right], \quad (2)$$

valid for a sphere, with spin waves propagating in a direction \hat{k} at angle θ_k to \vec{H} ; here $\omega_M = \gamma 4\pi M_s$. For the values $\omega_0 = 8.16 \times 10^9$ sec⁻¹, $\omega_M = 5.27 \times 10^9$ sec⁻¹, $\gamma = 17.58 \times 10^6$; $D = 5.4 \times 10^{-9}$ Oe cm² used in our experiment, ω_k is plotted in Fig. 2 for three angles: $\theta = 0^\circ$, $\theta = 90^\circ$, and $\theta = \theta_0 = 60.4^\circ$, the value for which $\omega_0 = \omega_k$ at $k = 0$; this is the largest angle for which ω_0 can equal ω_k . It is the nonlinear coupling between the uniform mode at ω_0 and spin

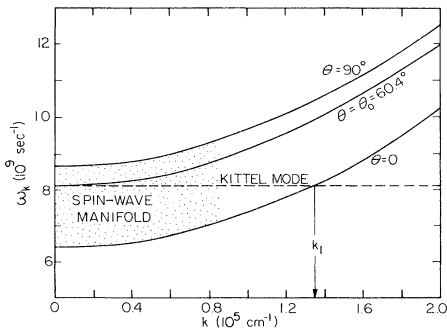


FIG. 2. Plot of spin-wave frequency ω_k vs wave vector k from Eq. (2), for experimental parameters used for Ga-YIG sphere. First instability occurs for spin waves traveling along the magnetic field ($\theta = 0$) with wave vector $k = k_1$, for which the spin-wave frequency becomes equal to the Kittel frequency ω_0 .

waves at ω_k that gives rise to the instabilities of interest, chiefly through the dipolar term.

Suhl, in an elegant analysis of the nonlinear coupling, found that an instability arises in first order [i.e., for terms of the form (uniform amplitude) \times (spin-wave amplitude)], if $\omega_0 = 2\omega_k$, i.e., one magnon of the uniform mode creates two spin-wave magnons. This could occur at saturation of the subsidiary resonance at $H_{res} \approx \frac{1}{2}H_0$, requiring $(\omega_0/2) > (\omega_0 - \omega_M/3)$. This condition is not satisfied in our experiment, i.e., half-frequency magnons lie outside the spin-wave manifold and cannot couple; this can be seen from Fig. 2. A first-order instability can also occur at saturation of the main resonance $H_{res} = H_0$ if $(\omega_M/3) > (\omega_0/2)$; again this condition is not satisfied under our experimental conditions.

We thus examine Suhl's second-order instability [i.e., (uniform amplitude)² \times (spin-wave amplitude), the so-called triple terms], leading to premature saturation of the main resonance, and requiring $\omega_0 = \omega_k$ and $H_{res} = H_0$, which can be achieved in our experiment, and is the only instability we consider further.

Suhl found that the lowest-threshold value of H_1 occurs for $\theta_k = 0$; from Eq. (2) the corresponding k value is given by

$$\gamma D k_1^2 = \omega_M/3. \quad (3)$$

This means that as the uniform mode resonance is saturated by increasing the H_1 field, the first instability to arise will excite spin waves at $\omega_k = \omega_0$ and $k = k_1$ in Fig. 2. These waves travel along H_0 in the spherical sample. This effect was observed by Damon¹ and by Bloembergen and Wang² as a weakening and broadening (premature saturation) of the resonance line at a rather low value of H_1 . Besides providing a quantitative explanation for the onset of premature saturation, Suhl's theory also predicted the detailed behavior of the spin system beyond threshold.

Because of the finite linewidth of the uniform mode, one may expect that this instability will excite spin waves with a spread $\Delta\omega_k$ and Δk of frequency and wave vector, which can be described as a spin-wave packet traveling with group velocity $v_g = d\omega_k/dk$. This can be calculated from Eq. (2), which, with $\omega_k = \omega_0$ for the instability of interest here, results in

$$v_g = \left(\frac{1}{2} \gamma D \omega_0 \right)^{1/2} \left\{ \left[-2 + \frac{2}{3} \beta - \beta \sin^2 \theta \pm (\beta^2 \sin^4 \theta + 4)^{1/2} \right] \times (\beta^2 \sin^4 \theta + 4)^{1/2} \right\}, \quad (4)$$

where $\beta \equiv \omega_M/\omega_0 = 0.64$ for our experiment. This expression gives the group velocity as a function of θ along the line $\omega_k = \omega_0$, the Kittel frequency, in the dispersion diagram of Fig. 2. For $\theta = 0$,

$$v_g = 2(\gamma D \omega_M/3)^{1/2} \text{ at } k = k_1, \quad (5)$$

with the value $v_g = 2.6 \times 10^4$ cm/sec for our experiment. For $\theta > 0$, but still small,

$$v_g \cong \left[\left(\frac{2}{3} - \sin \theta \right) (2\gamma D \omega_M) \right]^{1/2}, \quad (6)$$

showing that v_g decreases with increasing θ , and $v_g \rightarrow 0$ as $\theta \rightarrow \theta_0$, $k \rightarrow 0$ in Fig. 2.

The simplest example of a spin-wave packet is one com-

posed of a pair of spin waves $\omega_k + \Delta\omega_k$ and $\omega_k - \Delta\omega_k$, both excited by the uniform mode with $\Delta\omega_k/\omega_k \ll 1$.

Wang *et al.*⁵ suggested that standing-wave modes of this packet could be set up in a ferrite sample, in their case, a disc. For an isotropic sphere of radius R the normal electromagnetic modes are known to be given by spherical Bessel functions. Thomas and Komoriya⁶ assumed the spins are pinned at the spherical surface, so that the lowest normal mode will be the first zero of these functions $\pi = R \cdot \Delta k_0$, yielding a mode frequency

$$\omega_A = \Delta k_0 v_g = \pi v_g / R . \quad (7)$$

More generally, the spherical mode frequencies will be given by the zeros of the spherical Bessel functions of order zero, one, two, etc., given by $R \cdot \Delta k_0 = 3.141, 4.493, 5.763, 6.987, 8.182, \dots$ ¹⁷

These standing spin-wave packet oscillations would be manifest experimentally as a time modulation at ω_A of the magnetization, i.e., the detection of a modulation frequency ω_A in the signal voltage V_s , Fig. 1, since any oscillations of the spin waves will be coupled back into the uniform mode. This, in fact, is the explanation of the auto-oscillations of Wang *et al.*⁵ and Thomas and Komoriya.⁶

We conclude, then, that the excitation of the standing mode at ω_A is a spontaneous excitation of the nonlinear spin system, driven by the ferromagnetic resonance at a much higher frequency ω_0 . We experimentally find that this excitation displays chaotic dynamics. In this sense the spin system is analogous to, say, the excitation of convective loop frequencies in a fluid driven by a temperature gradient in Benard-Rayleigh convection.^{9,10}

IV. SIMPLE REVIEW OF CHAOTIC DYNAMICS

Although the nonlinear dynamics theory of Suhl, and of Gottlieb and Suhl¹⁸ for the parallel pumping case, do give detailed prediction of the spin-system behavior, more recently theories have appeared, e.g., Nakamura *et al.*¹⁹ and Ohta and Nakamura,²⁰ that view the dynamics as being controlled by a strange attractor in phase space, and the onset of instabilities as an example of a universal route to chaos.⁸ We take this viewpoint and examine the data in a manner to test these ideas, which we now review.

It is known that even complex systems, if sufficiently dissipative, can sometimes be modeled by simple low-order finite-difference equations. Consider a nonlinear periodic system with dynamical variable x , being driven by a control parameter A , for which x_{n+1} is some function $F(x_n, x_{n-1}, \dots, A)$, where the iterates x_n, x_{n+1} , are values at successive times separated by the period of the system. For the simplest case the return map function F is one-dimensional and quadratic:

$$x_{n+1} = 1 - Ax_n^2, \quad (8)$$

the logistic map.²¹ As A is increased, there is a threshold value $A = 0.75$, for which x_{n+1} becomes unstable and takes two alternating values; then four for larger A , etc. The system displays a cascade of period-doubling pitchfork bifurcations to an accumulation point $A = A^* = 1.4010 \dots$ where the period becomes infinite: this is the

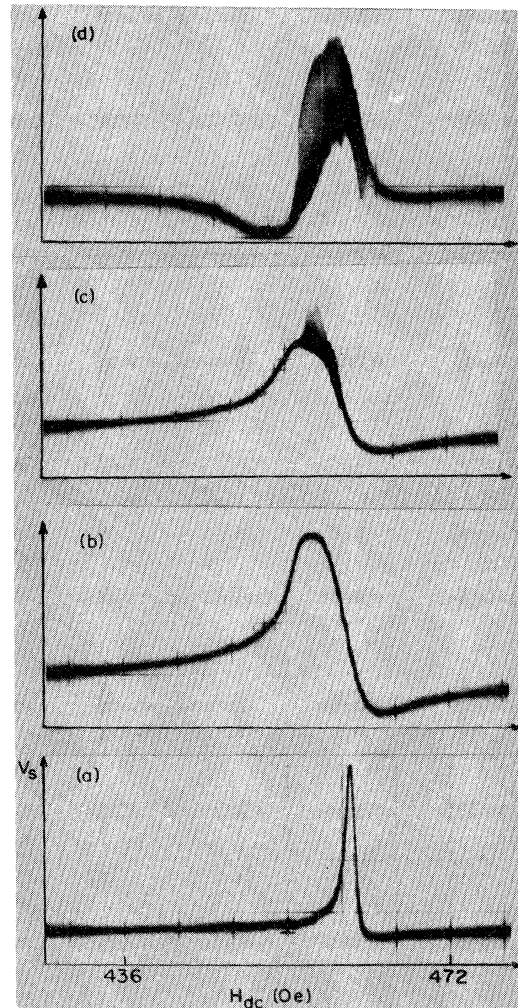


FIG. 3. Ferromagnetic resonance line shapes at $f_0 = 1.3$ GHz for a Ga-YIG sphere at increased values of driving field H_1 : (a) $H_1 = 1$ (relative units); (b) $H_1 = 30$; (c) $H_1 \approx 31$, showing onset of auto-oscillations; (d) $H_1 \approx 35$, fully developed oscillations.

transition to aperiodic or chaotic behavior. For $A > A^*$, aperiodic bands merge and there exist narrow periodic windows in a specific order and pattern.²² This model is quantified by the bifurcation convergence rate δ and pitchfork scaling parameter α computed by Feigenbaum.²³ Many other routes to chaos are possible, including intermittency²⁴ and quasiperiodicity.²⁵

Equation (8) is valid for systems with very large dissipation; it can be generalized into the two-dimensional Hénon map¹³ which allows for adjusted dissipation through a parameter B ,

$$x_{n+1} = 1 - Ax_n^2 + y_n, \quad (9a)$$

$$y_{n+1} = Bx_n. \quad (9b)$$

For $B = 0$, Eq. (9) reduces to the logistic map, while for

$|B|=1$ the mapping becomes area preserving, corresponding to a physical system which is conservative.

V. RESULTS AND INTERPRETATION

Figure 3 shows a series of ferromagnetic resonance line shapes in a Ga-YIG sphere of radius $R=0.047$ cm for increasing values of the driving field H_1 : Fig. 3(a), $H_1=1$ (relative units), low-power unsaturated resonance; Fig. 3(b), $H_1 \approx 30$, showing broadening and premature saturation; Fig. 3(c), $H_1 \approx 31$, at onset of instability and noisy oscillations; Fig. 3(d), $H_1 \approx 35$, more fully developed oscillations. To obtain a real-time signal of the oscillations, H_{dc} and f_0 are held at their center values, while the modulation field is set to zero, and $V_s(t)$ is photographed

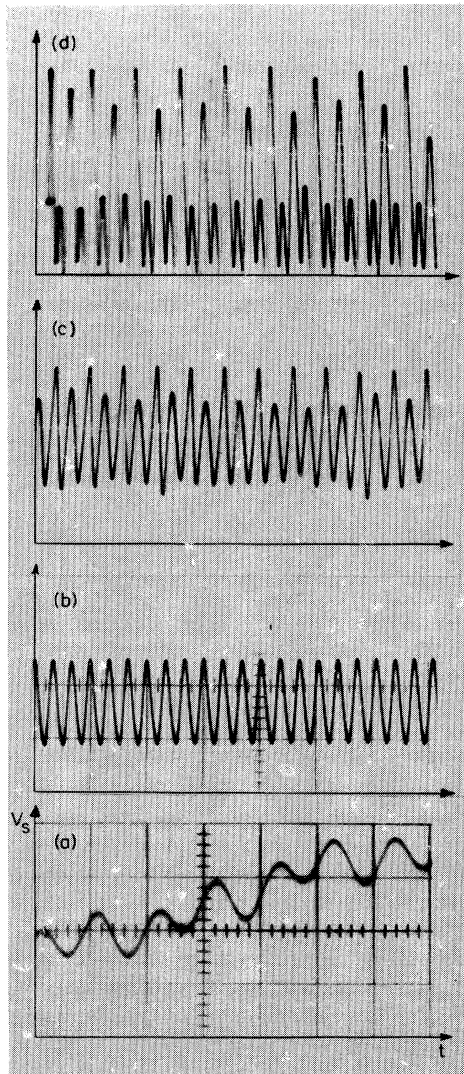


FIG. 4. Real-time signals, $V_s(t)$ vs t , for auto-oscillations: (a) at the H_1 value as in Fig. 3(c), auto-oscillation frequency $f_{A1} \approx 250$ kHz; (b) at higher H_1 , auto-oscillation frequency $f_{A2} \approx 16$ kHz; (c) at higher H_1 , bifurcation to $f_{A2}/2$; (d) bifurcation to $f_{A2}/4$.

with a single trace sweep, Fig. 4. The amplitude and stability depend on the sample crystal axes orientation, which was then chosen to optimize the oscillations.

These auto-oscillations had a well defined H_1 for their onset. Figure 4(a) shows the oscillations observed at the lowest value of H_1 ; they have a frequency of $f_{A1} \approx 250$ kHz. As H_1 was increased, these diminished in amplitude; other auto-oscillations as in Fig. 4(b) at the low frequency $f_{A2} \approx 16$ kHz were observed at higher H_1 [cf. Fig. 3(d)]. We interpret f_{A1} and f_{A2} as follows. In Sec. III we showed that the only instability possible for the parameters of our experiment is the second-order premature saturation of the main resonance. In fact, we do not observe any subsidiary resonance or instability at half field, $H_{res} \approx H_0/2$. Thus, we expect the lowest threshold to occur for $\theta_k=0$ at k_1 , Fig. 2, corresponding to the group velocity of Eq. (5). The lowest-frequency (zero-order) standing-wave packet mode will be given by Eq. (7), which

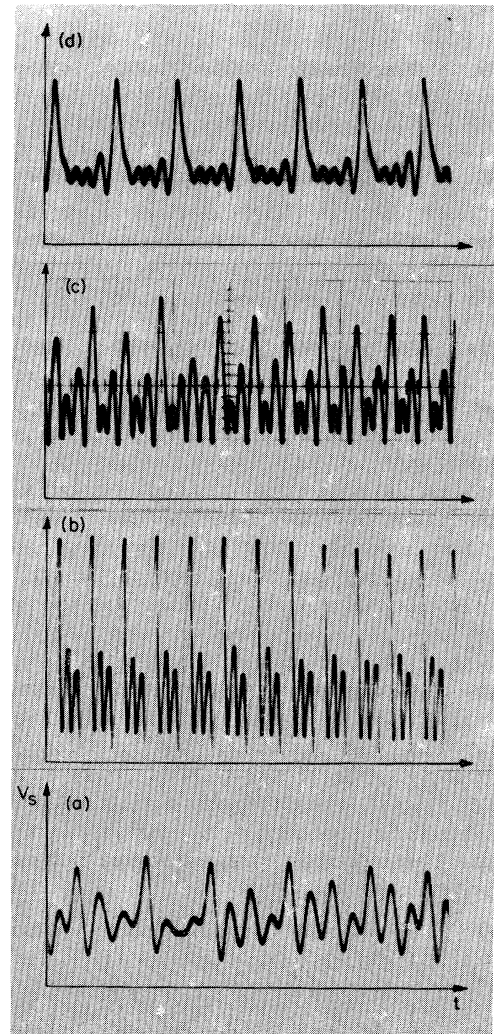


FIG. 5. Real-time signals, $V_s(t)$ vs t , for various values of H_1 : (a) chaos following Fig. 4(d); (b) period-3 auto-oscillations; (c) bifurcation to period 6; (d) period 4, but with different pattern from Fig. 4(d).

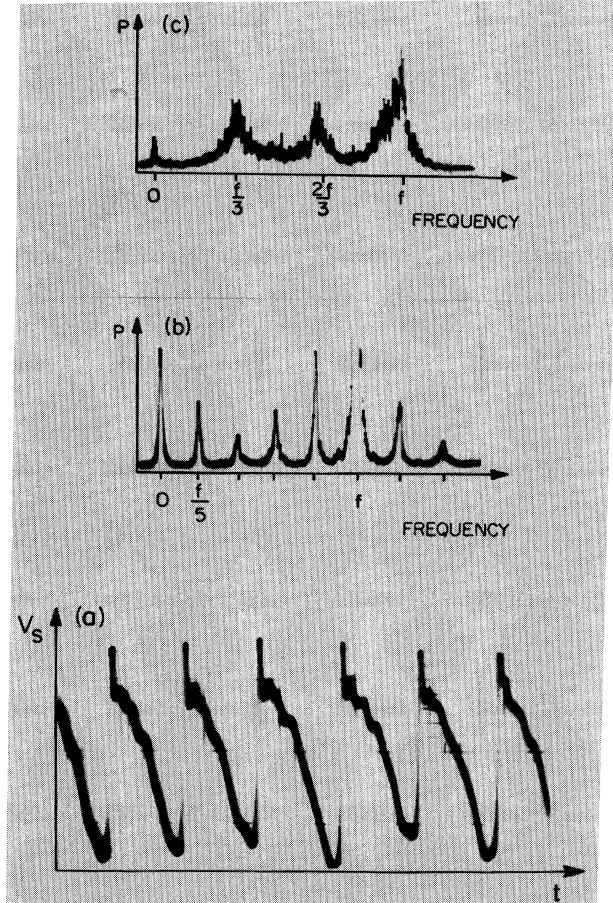


FIG. 6. (a) $V_s(t)$ vs (t) for a relaxation oscillation; (b) power spectra for a period-5 auto-oscillation, showing subharmonic components $f/5, 2f/5, \dots, f, 6f/5, \dots$; (c) power spectra for a noisy three-band attractor.

for radius $R = 0.047$ cm yields a frequency

$$f_A = \omega_A / 2\pi = (\gamma D \omega_M / 3)^{1/2} / R \quad (10)$$

approximately equal to 275 kHz. This value corresponds favorably with the observed $f_{A1} = 250$ kHz. Additional experiments with a Ga-YIG sphere of radius $R = 0.036$ cm showed the scaling $f_{A1} \propto 1/R$. Experiments with a pure YIG sphere, $R = 0.033$, and $4\pi M_s = 1750$ g showed weak auto-oscillations at 900 kHz, to be compared to 920 kHz predicted from Eq. (10). We conclude that this auto-oscillation is the standing-wave mode suggested by Wang *et al.*² and by Thomas and Komoriya⁶ at $\theta = 0^\circ$. The low-frequency oscillations at f_{A2} cannot be due to a higher-order mode at $\theta = 0$, and we ascribe them to the zero-order mode of Eq. (7) but with a small value of v_g at some angle θ^* such that

$$f_{A2} = \omega_A / 2\pi = v_g(\theta^*) / 2R. \quad (11)$$

The observed value $f_{A2} = 16$ kHz requires $v_g = 1.5 \times 10^3$ cm/sec, which can be obtained from Eq. (4) for $\theta = \theta^* = 60^\circ$, i.e., close to the value $\theta_0 = 60.4^\circ$ at which

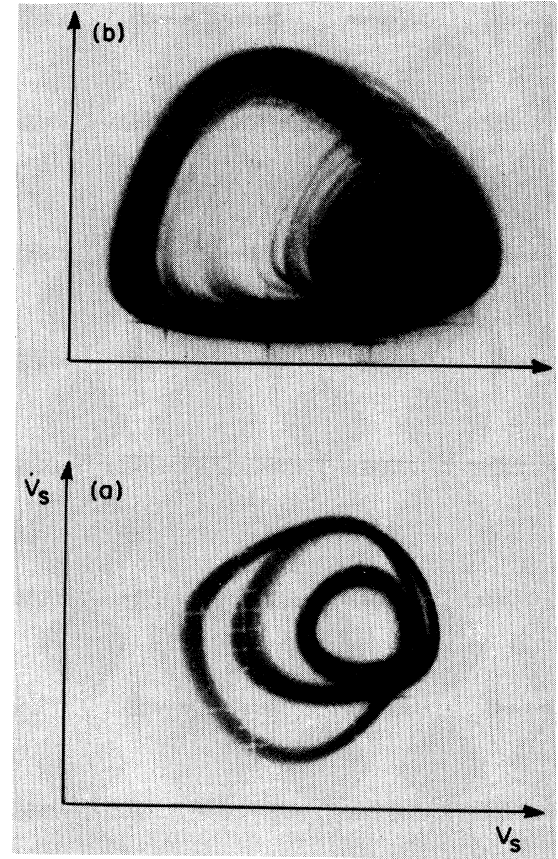


FIG. 7. Phase portraits, V_s vs \dot{V}_s , for (a) period-3 auto-oscillations, cf. Fig. 5(b); (b) chaos, cf. Fig. 5(a).

$k \rightarrow 0$, Fig. 2. We conclude that the strong auto-oscillations at f_{A2} are due to the lowest-order spherical Bessel function mode of a packet of spin waves of wave vector $k \approx 0$.

In further experiments we measured the lifetime of these oscillations at f_{A2} by pulsing off the H_1 field, finding an exponential decay with lifetime $\approx 10^3$ cycles. This indicates that this mode is only weakly coupled to other

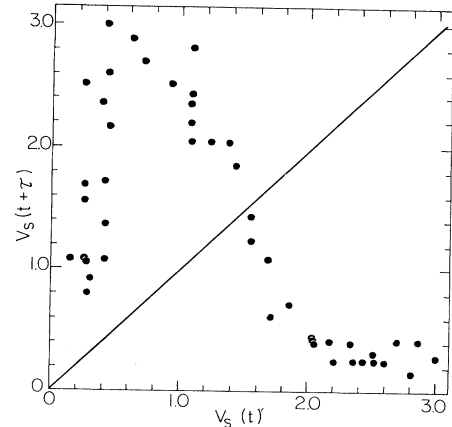


FIG. 8. Return map constructed from the chaotic state of Fig. 5(a). Here $\tau \approx 0.2T$.

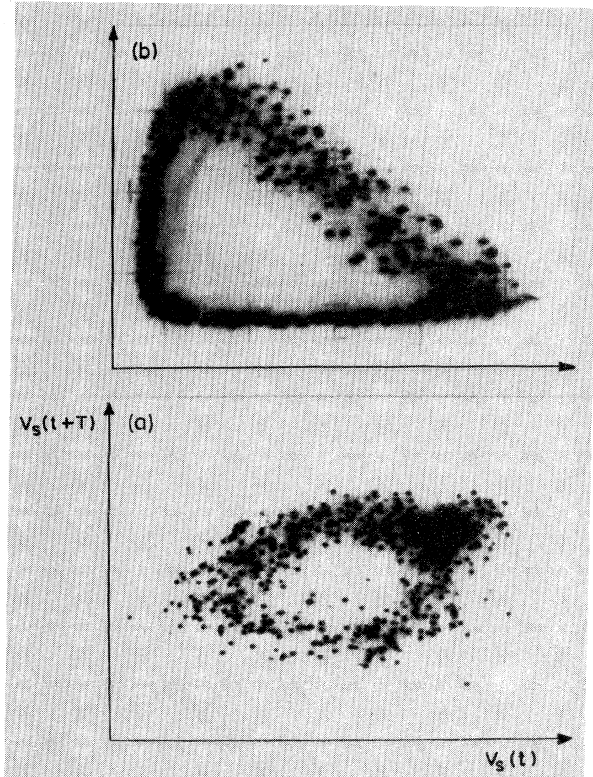


FIG. 9. Return map observed for period-1 auto-oscillations in a Ga-YIG sphere; (a) and (b) are for slightly different values of H_1 .

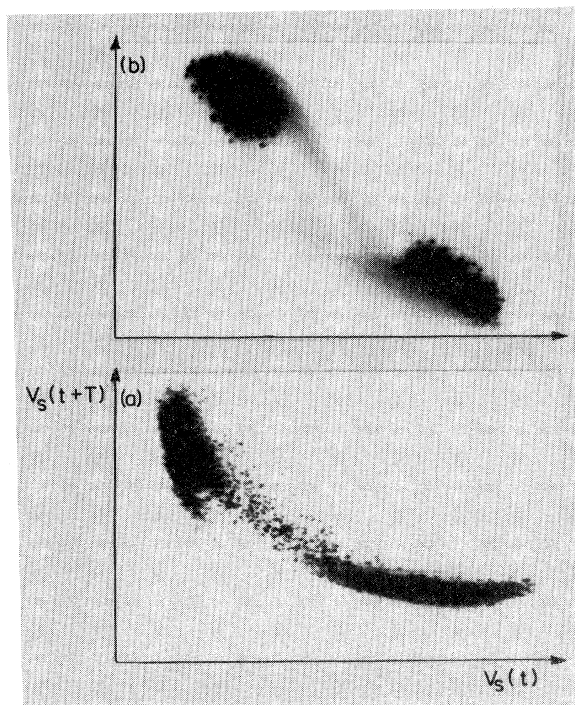


FIG. 10. Return map observed for period-2 auto-oscillations in Ga-YIG sphere: (a) onset of period-2 bifurcation; (b) period 2.

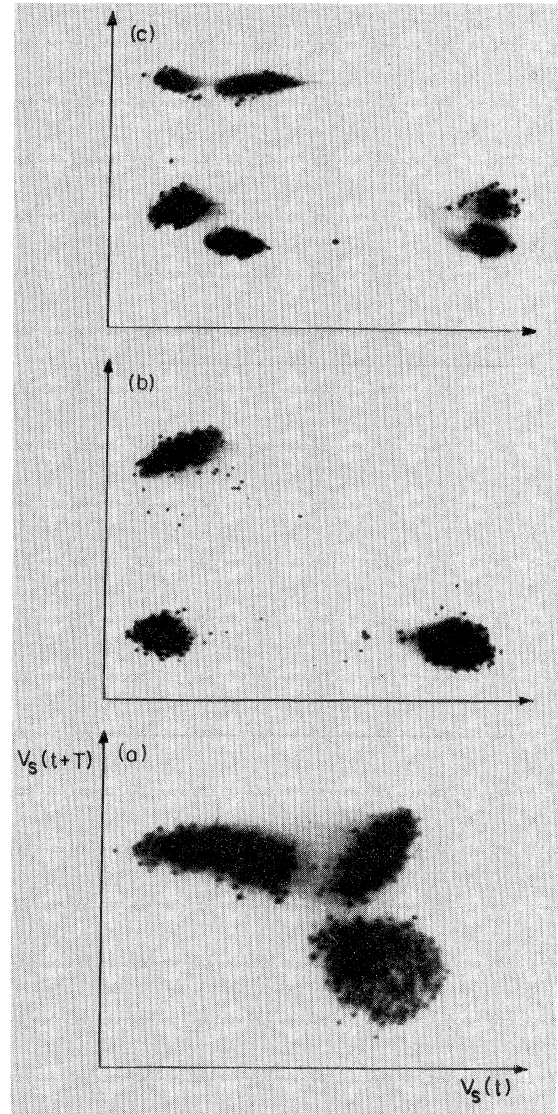


FIG. 11. Return map observed for period-3 auto-oscillations: (a) onset of period-3 oscillations; (b) clear period 3; (c) bifurcation to period 6 at higher value of H_1 .

modes and to the lattice phonons. Summarizing, the spin system when strongly pumped at the main resonance at 1.3 GHz spontaneously excites a packet of spin waves ($k \approx 0$) which have a dimensional resonance at the relatively low frequency $f_{A2} \approx 16$ kHz. These oscillations were found to show chaotic dynamics.

This is shown most simply by a sequence of f_{A2} oscillation signals $V_s(t) \propto \dot{M}(t)$, obtained at increased H_1 values. These first appear in Fig. 4(b) as a sine wave at $f_{A2} = 16$ kHz. There is a higher threshold at which the signal bifurcates to period 2, Fig. 4(c); then to period 4, Fig. 4(d). Further increase of H_1 leads to onset of a "noisy" aperiodic signal we call chaos, Fig. 5(a), although we have not proved experimentally that it is deterministic. However, there is no reason why random (e.g., thermal) noise should

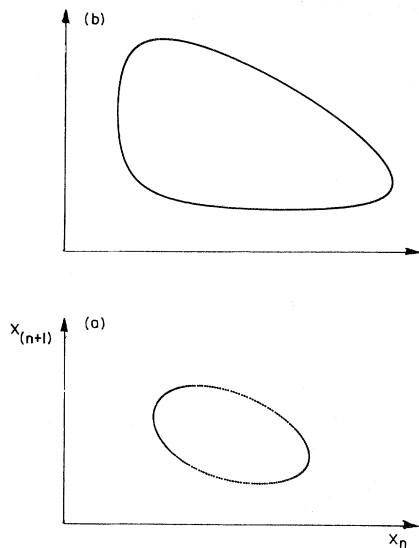


FIG. 12. Return map, x_{n+1} vs x_n , computed from Eq. (9) for $B = -1$: (a) $A = 0.95$, $x_0 = y_0 = 0.4$; (b) $A = 0.95$, $x_0 = y_0 = 0.3$; cf. data, Fig. 9.

abruptly increase between Fig. 4(d) and Fig. 5(a). We also observed a periodic state of period 3, Fig. 5(b), which bifurcates to period 6, Fig. 5(c), and then becomes chaotic. Other periodic states observed are period 5 and period 4, Fig. 5(c), with a visitation pattern different from that of Fig. 4(d). Although the overall behavior seems roughly similar to that observed in p - n junctions and in other non-linear systems, the spin system is much less stable and the behavior less reproducible than in p - n junctions. There are more parameters: H_0 , f_0 , H_1 , crystal orientation, and temperature. Fluctuations in these (none are highly stabilized) give drifts and even jumps from one dynamical state to another. This gives the appearance of intermittency, however, probably not that of Manneville and Pomeau.²⁴ We also observe a strong hysteresis, i.e., a dependence of the chaotic dynamics on the direction in which H_0 and f_0 are set to resonance, and also on whether H_1 is increased or decreased toward a threshold value. The system seems to have several attractors with quite different behavior. That described above is probably the most characteristic and reproducible. Another, quite different signal shape is shown in Fig. 6(a), reminiscent of relaxation oscillations in general; in fact, Hartwick *et al.*⁴ in their discovery of auto-oscillations described them as relaxation oscillations. We believe that these are distinct phenomena but have not investigated their possibly chaotic dynamics.

Power spectra were measured by a frequency-scanning spectrum analyzer. The results confirm the signal periods measured above from real-time analysis. Figure 6(b) is the spectrum for a period-5 oscillation, showing spectral components at $f/5, 2f/5, \dots, f, 6f/5, 7f/5, \dots$ and very small peaks at $f/10, \dots$. Figure 6(c) is the spectrum for a noisy three-band attractor near the period-3 window. The chaotic state, Fig. 5(a), showed a wide-band spectrum with a broad peak at f_{A2} . By plotting $V_s(t) vs V_s(t)$ on an oscilloscope, real-time phase portraits were obtained: Fig.

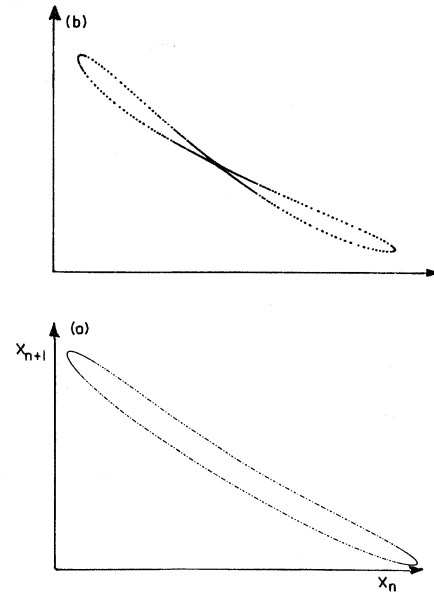


FIG. 13. Return map computed from Eq. (9) for $B = -1$: (a) $A = 3.02$, $x_0 = y_0 = 0.3325$; (b) $A = 3.1$, $x_0 = y_0 = 0.33$; cf. data, Fig. 10.

7(a), period-3 window, Fig. 7(b), chaos.

More detailed information about the system can be obtained from a return map: a plot of $V_s(t + \tau) vs V_s(t)$, when τ is some fixed time. This can then be compared to a theoretical model, e.g., the logistic map, Eq. (8), for which $x_{n+1} vs x_n$ is a parabola. The return map constructed from Fig. 5(a) is shown in Fig. 8; it is, very crudely, a single-humped curve with a quadratic maximum. However, other data yielded the rather different return

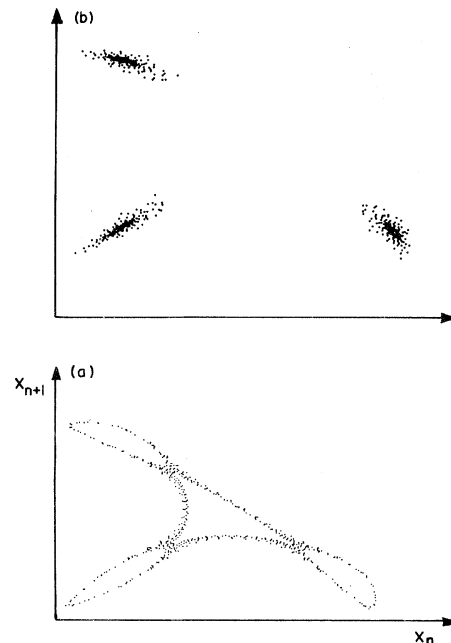


FIG. 14. Return map computed from Eq. (9) for $B = -1$: (a) $A = 1.0385$, $x_0 = y_0 = 0.5$; (b) $A = 1.058$, $x_0 = y_0 = 0.5$; cf. data, Fig. 11.

maps of Figs. 9–11. These were obtained by using a zero crossing detector to give a pulse train of approximately period T ; this strobed a sample-and-hold circuit which then plotted $V_s(t+T)$ vs $V_s(t)$ directly on an oscilloscope. It was not known if the system dynamics, and the attractor, is the same for Fig. 8 and for Figs. 9–11, which do not appear to be modeled by the logistic map. In fact, these return maps appear to be similar to those computed from the Hénon map, Eq. (9), for $B \approx -1$ (i.e., for a nearly conservative system) shown in Figs. 12–14, for the values $A=0.95, 3.02,$ and 1.04 , corresponding to periods 1, 2, and 3, respectively. We have no more detailed experimental reasons, nor any theoretical reasons, for believing that the spin-system dynamics is modeled by the Hénon map, but merely note this similarity.

To summarize, a reexamination of the Suhl spin-wave instabilities in a Ga-YIG sphere has shown that there exists a very low-frequency auto-oscillation, not previously

reported, corresponding to the lowest spherical dimensional resonance of a packet of spin waves of small wave number. This displays period doubling, chaos, and periodic windows, as well as hysteresis, relaxationlike oscillations, and probably several different attractors. Some of the behavior is characterized by a single-humped return map. Other behavior yields maps qualitatively like the Hénon quadratic map for the nearly conservative case, consistent with the observed long lifetime of this dimensional mode. These results show that the auto-oscillations of spin waves have many similarities to instabilities found in fluid dynamics and other nonlinear systems.

ACKNOWLEDGMENTS

We acknowledge with much thanks helpful conversations with Alan N. Portis and Robert M. White. One of us (C.J.) acknowledges support by the Miller Institute for Basic Research in Science.

-
- ¹R. W. Damon, *Rev. Mod. Phys.* **25**, 239 (1953).
²N. Bloembergen and S. Wang, *Phys. Rev.* **93**, 72 (1954).
³H. Suhl, *J. Phys. Chem. Solids* **1**, 209 (1957).
⁴T. S. Hartwick, E. R. Peressini, and M. T. Weiss, *J. Appl. Phys.* **32**, 223S (1961).
⁵S. Wang, G. Thomas, and Ta-lin Hsu, *J. Appl. Phys.* **39**, 2719 (1968).
⁶G. Thomas and G. Komoriya, *J. Appl. Phys.* **66**, 883 (1975).
⁷For a review of the extensive Soviet work, see V. E. Zakharov, V. S. L'vov, and S. S. Starobinets, *Usp. Fiz. Nauk.* **114**, 609 (1974) [*Sov. Phys.—Usp.* **17**, 896 (1975)].
⁸For a review, see, e.g., J.-P. Eckmann, *Rev. Mod. Phys.* **53**, 643 (1981).
⁹A. Libchaber and A. Maurer, *Nonlinear Phenomena at Phase Transitions and Instabilities, Proceedings of a NATO Advanced Study Institute, Geilo, Norway, 1981*, edited by T. Risti (Plenum, New York, 1982), p. 259.
¹⁰J. P. Gollub and S. V. Benson, *J. Fluid Mech.* **100**, 449 (1980).
¹¹J. Testa, J. Perez, and C. Jeffries, *Phys. Rev. Lett.* **48**, 714 (1982); C. Jeffries and J. Perez, *Phys. Rev. A* **26**, 2117 (1982).
¹²R. H. Simoyi, A. Wolf, and H. L. Swinney, *Phys. Rev. Lett.* **49**, 245 (1982).
¹³M. Hénon, *Commun. Math. Phys.* **50**, 69 (1976).
¹⁴C. Kittel, *Introduction to Solid State Physics*, 5th ed. (Wiley, New York, 1976), Chaps. 15 and 16.
¹⁵C. Kittel, *Phys. Rev.* **71**, 270 (1947).
¹⁶A. M. Clogston, H. Suhl, L. R. Walker, and P. W. Anderson, *J. Phys. Chem. Solids* **1**, 129 (1957).
¹⁷*Handbook of Mathematical Functions*, U. S. Natl. Bur. Stand. (Appl. Math. Ser. No. 55), edited by M. Abramowitz and I. A. Stegun (U.S. GPO, Washington, D. C., 1965), p. 467.
¹⁸P. Gottlieb and H. Suhl, *J. Appl. Phys.* **33**, 1508 (1962).
¹⁹K. Nakamura, S. Ohta, and K. Kawasaki, *J. Phys. C* **15**, L143 (1982).
²⁰S. Ohta, and K. Nakamura, *J. Phys. C* (to be published).
²¹R. M. May, *Nature (London)* **261**, 459 (1976).
²²N. Metropolis, M. L. Stein, and P. R. Stein, *J. Comb. Theory, Ser. A* **15**, 25 (1973).
²³M. J. Feigenbaum, *J. Stat. Phys.* **19**, 25 (1978).
²⁴P. Manneville and Y. Pomeau, *Phys. Lett.* **75A**, 1 (1979).
²⁵D. Ruelle and F. Takens, *Commun. Math. Phys.* **20**, 167 (1971).

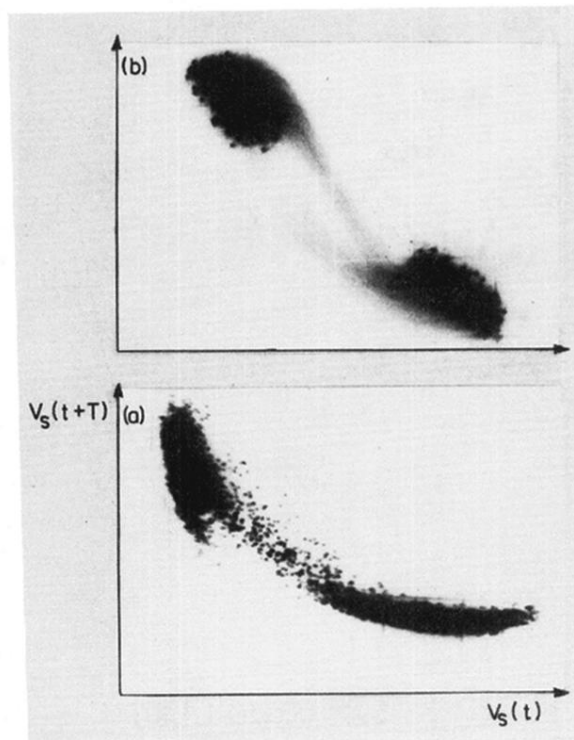


FIG. 10. Return map observed for period-2 auto-oscillations in Ga-YIG sphere: (a) onset of period-2 bifurcation; (b) period 2.

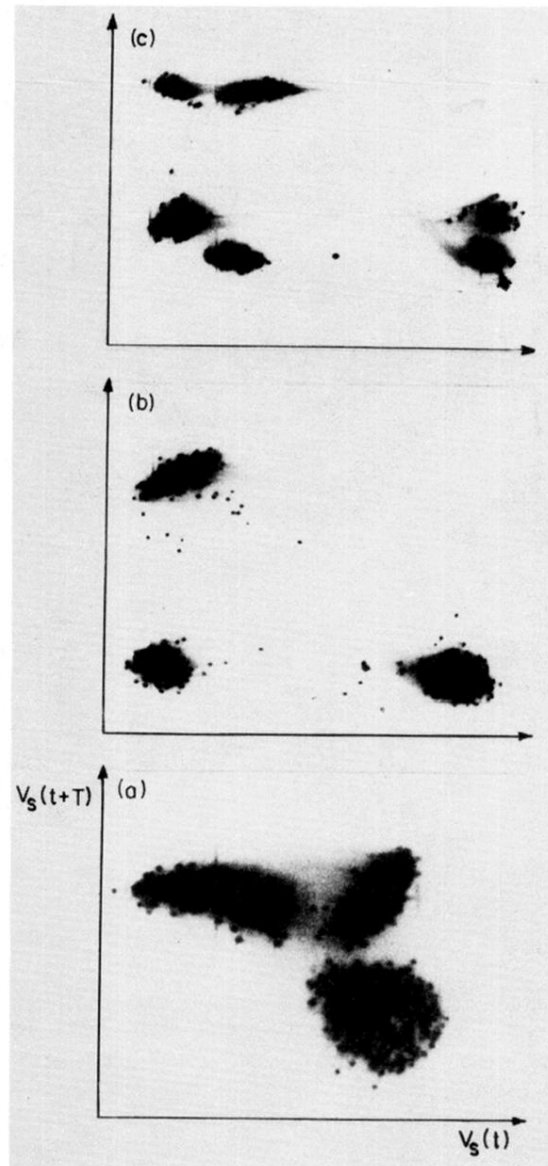


FIG. 11. Return map observed for period-3 auto-oscillations: (a) onset of period-3 oscillations; (b) clear period 3; (c) bifurcation to period 6 at higher value of H_1 .

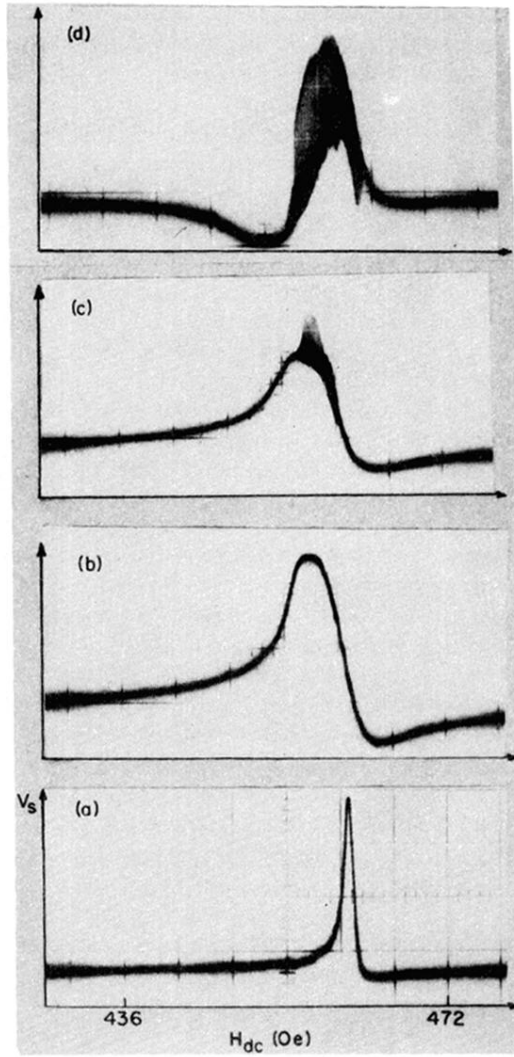


FIG. 3. Ferromagnetic resonance line shapes at $f_0=1.3$ GHz for a Ga-YIG sphere at increased values of driving field H_1 : (a) $H_1=1$ (relative units); (b) $H_1=30$; (c) $H_1 \cong 31$, showing onset of auto-oscillations; (d) $H_1 \approx 35$, fully developed oscillations.

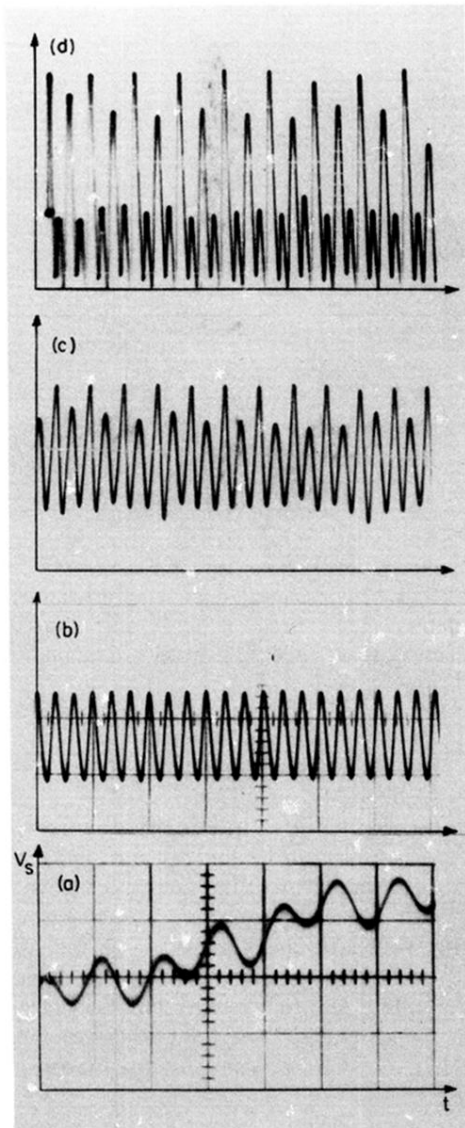


FIG. 4. Real-time signals, $V_s(t)$ vs t , for auto-oscillations: (a) at the H_1 value as in Fig. 3(c), auto-oscillation frequency $f_{A1} \approx 250$ kHz; (b) at higher H_1 , auto-oscillation frequency $f_{A2} \approx 16$ kHz; (c) at higher H_1 , bifurcation to $f_{A2}/2$; (d) bifurcation to $f_{A2}/4$.

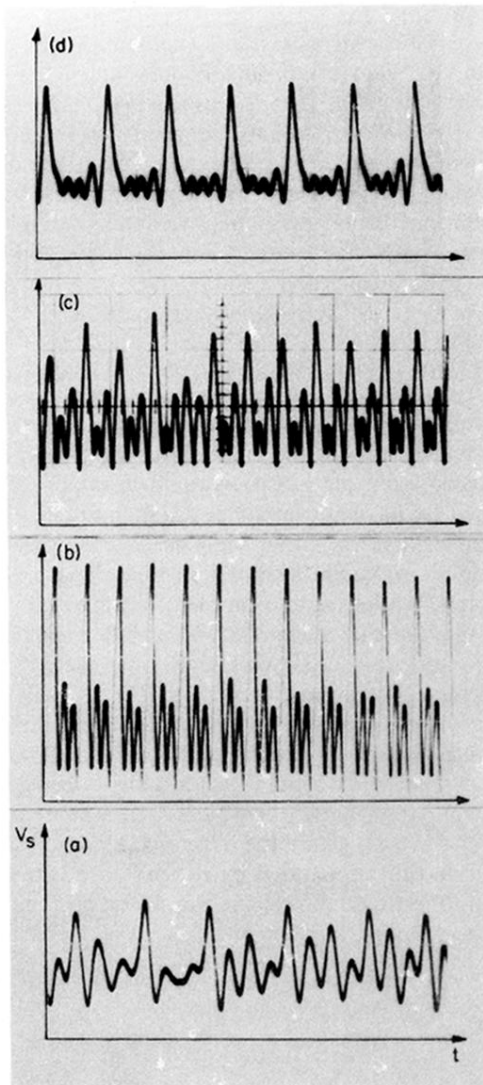


FIG. 5. Real-time signals, $V_s(t)$ vs t , for various values of H_1 : (a) chaos following Fig. 4(d); (b) period-3 auto-oscillations; (c) bifurcation to period 6; (d) period 4, but with different pattern from Fig. 4(d).

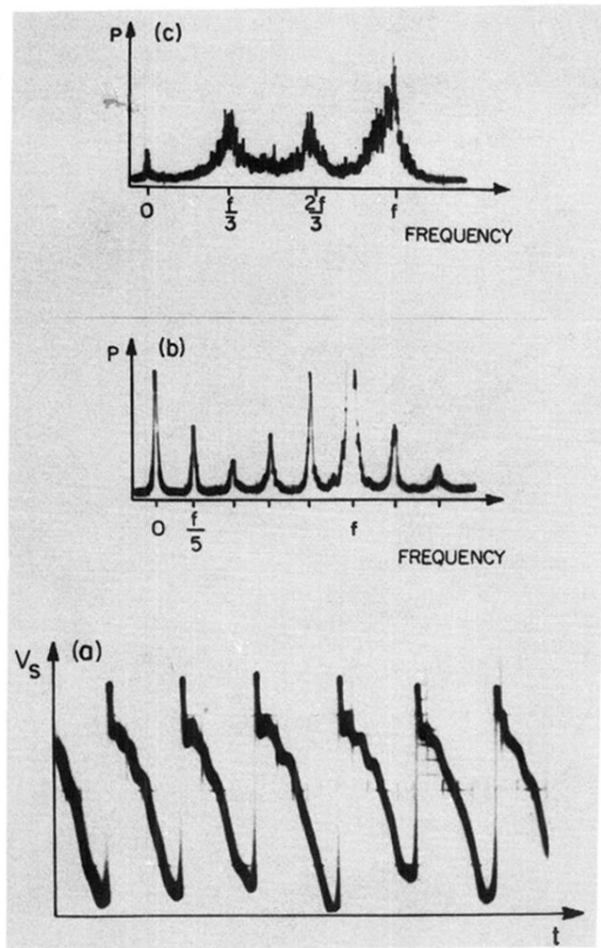


FIG. 6. (a) $V_s(t)$ vs (t) for a relaxation oscillation; (b) power spectra for a period-5 auto-oscillation, showing subharmonic components $f/5, 2f/5, \dots, f, 6f/5, \dots$; (c) power spectra for a noisy three-band attractor.

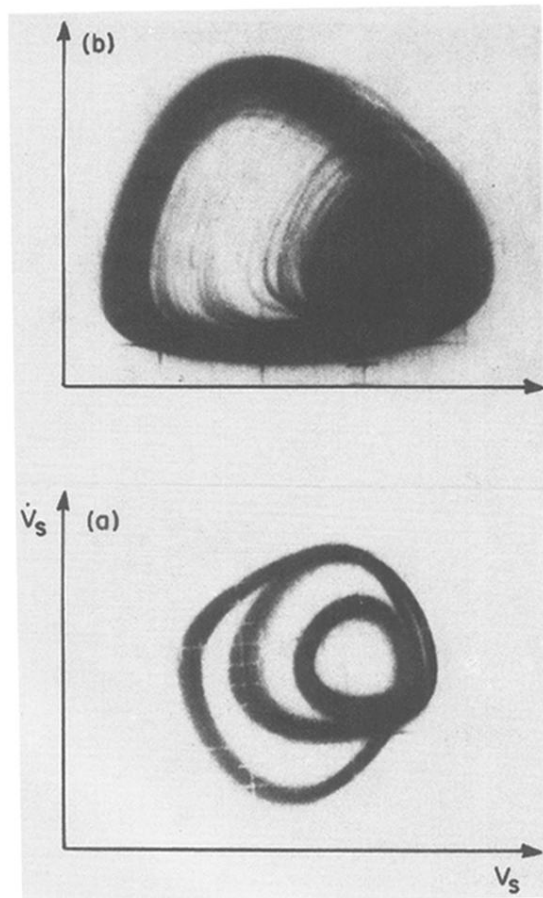


FIG. 7. Phase portraits, V_s vs \dot{V}_s , for (a) period-3 auto-oscillations, cf. Fig. 5(b); (b) chaos, cf. Fig. 5(a).

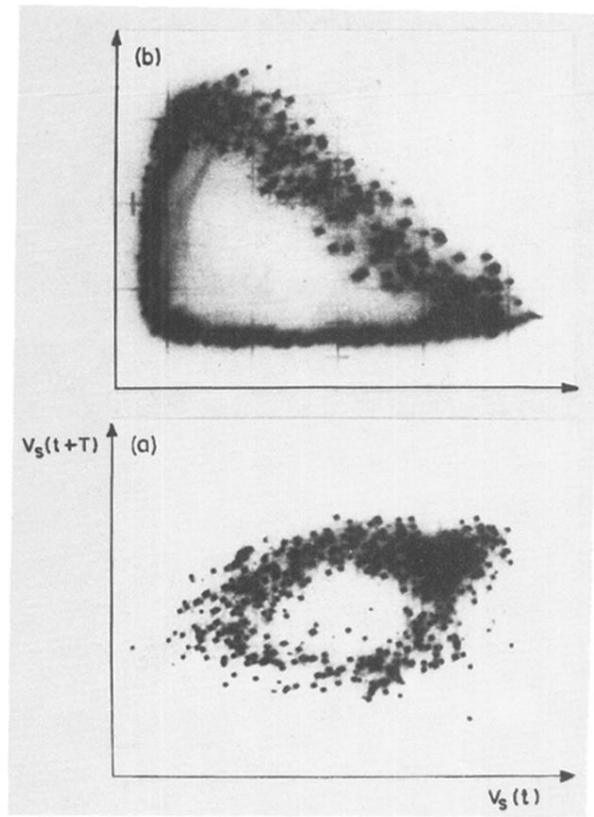


FIG. 9. Return map observed for period-1 auto-oscillations in a Ga-YIG sphere; (a) and (b) are for slightly different values of H_1 .